Zuerst erschienen in: Solid State Ionics 82 (1995), 95-106

# Determination of local potentials in mixed conductors – two examples

C. Rosenkranz, J. Janek *

*Institut für Physikalische Chemie und Elektrochemie and Sonderforschungsbereich 173 der Universität Hannover, Callinstr. 3-3A, 30167 Hannover, Germany*

**Abstract**

Two basic experiments for the measurement of local (electro-)chemical potentials in crystalline mixed conductors, which are exposed to external forces, are reported. (a) The profile of the chemical potential of silver metal in a Wagner–Hebb polarization cell Ag | AgBr | Pt is measured by means of local potential probes. Deviations from calculated profiles are discussed in terms of either a possible electronic overvoltage at the anodic interface AgBr | Pt or a change of the defect structure of AgBr in the region near the anode. (b) In a second experiment, the ionic overvoltage at an interface AgBr | AgCl is determined, again by means of local potential probes.

*Keywords:* Chemical potential profile; Mixed conductors; Overvoltage

## 1. Introduction

Fluxes of charge and matter in the crystalline state are driven by local gradients of respective thermodynamic potentials. Accordingly, for a complete quantitative description of transport processes and the determination of transport coefficients, both local fluxes and potential gradients have to be measured. In principle, this task can be solved by the use of local potential probes which, for the purpose of an acceptable spatial resolution, have to be miniaturized [1]. In this respect, a particular problem is the investigation of transport processes across interfaces between crystalline phases. From a macroscopic point of view, the driving forces for transport across phase boundaries are step-like. Therefore, by the use of local probes, these driving forces can be inferred from the extrapolation of the thermodynamic potentials within the bulk phases to the position of the interface (e.g., see [2,3]).

The intention of the present study is to report two basic experiments for the measurement of local potentials in ionic crystals and to discuss the results in respect of the kinetics of particular interfaces. In the first experiment, a conventional Wagner–Hebb polarization cell Ag | AgBr | Pt was constructed, with eight thin Pt-probes distributed along the AgBr crystal for the measurement of the local chemical potential of silver during the polarization experiments (see Fig. 1). Depending on the applied polarization volt-

* Corresponding author: Tel.: (0511) 762-5298, Fax: (0511) 762-4009 E-Mail: JANEK@MBOX.PCI.UNI-HANNOVER.DE.

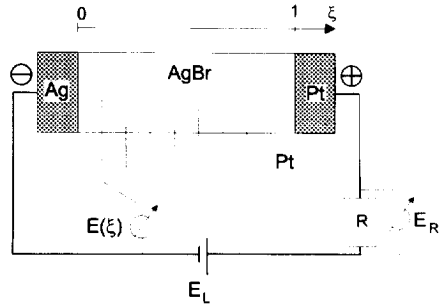


Fig. 1. Electrical circuit of the polarization cell Ag | AgBr | Pt.

age, characteristic profiles of the chemical potential are established within the crystal, which can be used for an evaluation of the local (i.e. activity dependent) electronic conductivity [4].

The second experiment is based on the measurement of local potentials in a heterogeneous transference cell Ag | AgCl | AgBr | Ag (see Fig. 2). As discussed extensively by Schmalzried and coworkers [5,6] in the context of internal reactions at interfaces, the discontinuity in transport properties across an interface AX | AY between two mixed conductors may lead to a deviation of the chemical potentials of the components at the interface from values at the electrode boundaries (which are usually fixed by metal A to a reference potential $\mu_A^0$ during current load). One aspect of the description of such transference cells, which is not predictable a priori, concerns possible electronic and ionic overvoltages at the interfaces. From the extrapolation of our measured potential profiles, we obtain information on the ionic overvoltages within the transference cell.

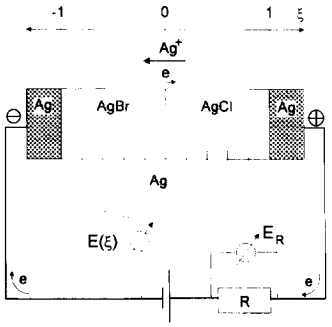


Fig. 2. Electrical circuit of the transference cell Ag | AgBr | AgCl | Ag.

## 2. Formal considerations

For the study of transport processes in mixed (ionic/electronic) conductors, basically two types of potential probes can be applied: (a) Inert metals (or other exclusively electronic conductors) can be used for probing the electrochemical potential $\tilde{\mu}_{e^-}$ of the electronic charge carriers, and (b), solid electrolytes can be used for probing the electrochemical potential $\tilde{\mu}_{A^{z+}}$ (or $\tilde{\mu}_{X^{z-}}$) of ionic charge carriers. The measurement of the chemical potential of compounds generally requires the simultaneous use of both probe types (e.g., $\Delta\mu_A = \Delta\tilde{\mu}_{A^{z+}} + z_A\Delta\tilde{\mu}_{e^-}$). Exceptions are measurements of chemical potentials of components in galvanic cells with partially blocked fluxes. Thus, in cells with ion-blocking electrodes, e.g., Wagner–Hebb polarization cells, the measurement of $\Delta\tilde{\mu}_{e^-}$ is sufficient for the determination of $\Delta\mu_A$ ($\Delta\mu_A \cong z_A\Delta\tilde{\mu}_{e^-}$), and in cells with electron blocking electrodes ($\Delta\tilde{\mu}_{e^-} = 0$) the measurement of $\Delta\tilde{\mu}_{A^{z+}}$ is sufficient for the determination of $\Delta\mu_A$ ($\Delta\mu_A \cong \Delta\tilde{\mu}_{A^{z+}}$).

In addition, the application of (electro-)chemical probes reversible for both ionic and electronic charge carriers in mixed ionic/electronic conductors is possible [7]. But in this case the interpretation of the measured signal needs more care since the electrode potential depends on two exchange processes. However, for the determination of $\Delta\tilde{\mu}_{A^{z+}}$, probes of metal A can be used, but are in principle reasonable only for the special case of a chemical homogeneous system ($\Delta\mu_A = 0$) with small electronic transference number ($t_{e^-} \ll t_{A^{z+}}$) [7]. In case of a nonvanishing $\Delta\mu_A$ the diffusion potential gives rise to an additional probe signal, which disturbs the measurement of $\Delta\tilde{\mu}_{A^{z+}}$.

### *2.1. Local electronic potential probes in a polarization cell*

The formal treatment of polarization cells of the type A | AX | Me with an ion-blocking anode Me was first reported by Hebb and Wagner [8,9] for $Ag_2S$ and was later used by several authors for the study of other mixed conductors [10–12]. Thus, we will only summarize those relations which are important in the context of our own experiments.

In the steady state of polarization the ionic flux in the compound AX should be blocked completely, i.e. no decomposition takes place at the blocking anode. The applied electric potential difference $E_L$ between the platinum anode and the reversible silver cathode is related to the steady state current density $i_{el}$ by Wagner's equation [8] for the one-dimensional case,

$$i_{el} = \frac{RT}{LF}\left\{\sigma_{e^-}^0\left[1 - \exp\left(-\frac{E_L F}{RT}\right)\right] + \sigma_{h^\cdot}^0\left[\exp\left(\frac{E_L F}{RT}\right) - 1\right]\right\}, \quad (1)$$

where $\sigma_{e^-}^0$ and $\sigma_{h^\cdot}^0$ denote the partial conductivities of electrons and electron holes in AX for the case of equilibrium with metal A ($a_A = 1$). The length of the crystal is denoted by $L$, $R$ represents the gas constant and $F$ Faraday's constant. In the special case of predominant hole conductivity Eq. (1) simplifies to:

$$i_{h^\cdot} = \frac{RT}{LF}\left\{\sigma_{h^\cdot}^0\left[\exp\left(\frac{E_L F}{RT}\right) - 1\right]\right\}. \quad (2)$$

For the derivation of Eq. (1), negligible overvoltages are assumed at the electrodes. In other words, the local electrochemical equilibria

$$\tilde{\mu}_{e^-}(\mathrm{Pt}) = \tilde{\mu}_{e^-}(\mathrm{AX}) \quad (3)$$

and

$$\tilde{\mu}_{e^-}(\mathrm{A}) = \tilde{\mu}_{e^-}(\mathrm{AX}) \quad (4)$$

are assumed at the blocking platinum anode and the reversible cathode, respectively. As the ionic flux is blocked in the steady state of polarization ($j_{A^+} = 0$), the driving force for the metal ion flux vanishes everywhere,

$$\frac{\partial \tilde{\mu}_{A^+}}{\partial x} = 0, \quad (5)$$

and with the assumption of a negligible gradient in the chemical potential of the ions,

$$\frac{\partial \mu_{A^+}}{\partial x} \cong 0, \quad (6)$$

one generally concludes for the ideally polarized crystal that the gradient of the electric potential $\nabla\varphi$ vanishes everywhere, i.e.

$$\frac{\partial \varphi}{\partial x} \cong 0. \quad (7)$$

Thus, the gradient of the chemical potential of the metal component, $\mu_A$, is just the gradient of the chemical potential of the electrons, $\mu_{e^-}$:

$$\frac{\partial \mu_A}{\partial x} = \frac{\partial \tilde{\mu}_{e^-}}{\partial x} \cong \frac{\partial \mu_{e^-}}{\partial x}. \quad (8)$$

It has to be emphasized that Eq. (6) is only valid for systems with small ranges of homegeneity and high intrinsic disorder (e.g. AgBr). Additionally, Eq. (6) is not a priori valid in space charge regions near electrodes.

Eqs. (7) and (8) state that the electronic charge carriers in an ideally polarized crystal are only driven by their concentration gradients, since no inner electric field exists in the crystal. Independent of this consideration, the potential difference $E(\xi)$ measured between a Pt-probe at a relative position $\xi = (x/L)$ and the silver cathode ($\xi = 0$) always reflects

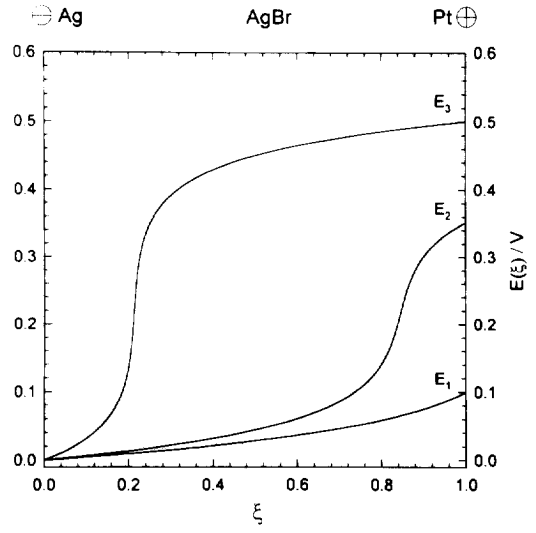


Fig. 3. Calculated chemical potential profile in the polarization cell Ag|AgBr|Pt.

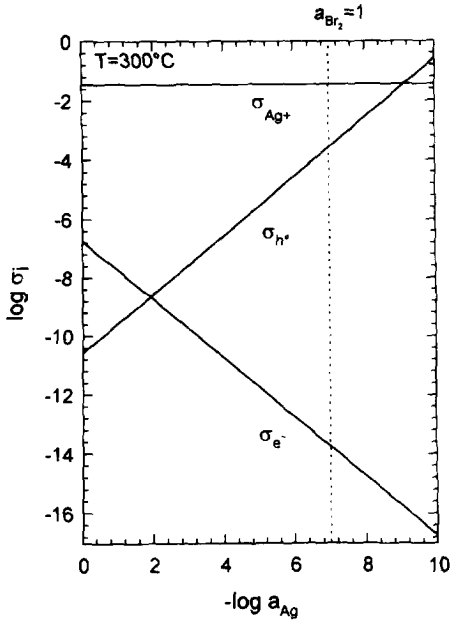


Fig. 4. Calculated conductivities of the electrons and hole versus the bromine activity in AgBr at 300°C.

the chemical potential in the compound at $\xi$ relative to the chemical potential of the silver cathode

$$E(\xi) = -\frac{1}{F}\left[\mu_A(\xi) - \mu_A^0\right]. \qquad (9)$$

Accordingly, by this definition the cell voltage $E_l$ in Eq. (1) equals $E$ ($\xi = 1$) and $\nabla\mu_A = -F\nabla E(\xi)$. Using Eq. (1), replacing $E_L$ and $L$ by $E(\xi)$ and $\xi$, and inserting reference values for the partial electronic and hole conductivities $\sigma_e^0$ and $\sigma_h^0$ [10,13], the profile of $E(\xi)$ and thus the chemical potential of silver metal $\mu_A(\xi)$ in AX can be calculated as a function of the relative position $\xi$ in the specimen as depicted in Fig. 3 for different current densities.

The chemical potential of the metal (i.e. the chemical potential of the electrons) develops a characteristic s-shaped profile with increasing cell voltage $E_L$, which directly relates to the local electronic conductivity and its dependence on the chemical potential of the metal (see Fig. 4). An inflection point denotes the minimum in the electronic conductivity, at which the electronic conduction changes from n- to p-type. The relative position of the inflection point moves towards the reversible silver cathode with increasing polarization of the sample, indicating the growing p-character of the crystal. The electronic partial conductivity decreases with decreasing silver activity from its reference value $\sigma_e^0$ ($a_A = 1$) with a slope of $\partial \ln \sigma_e / \partial \ln a_A = -1$. The electron hole partial conductivity increases with decreasing silver activity from its reference value $\sigma_h^0$ ($a_A = 1$) with a slope of $\partial \ln \sigma_h / \partial \ln a_A = 1$. At a silver activity of approximately $a_A = 0.01$ the conductivity for holes equals the conductivity for electrons.

Usually, the electronic partial conductivities are derived from an analysis of the current-voltage relation of polarization cells (e.g., [10]). Alternatively, the partial electronic conductivity can be calculated from the ratio of the local potential gradient and the externally measured current density ($i_{el} = I_A/A$, with $A$ = the cross sectional area of the crystal):

$$\sigma_{el}(\xi) \equiv \sigma_e(\xi) + \sigma_h(\xi) = \frac{i_{el}}{\nabla E(\xi)}. \qquad (10)$$

Thus, at least theoretically, from a single measurement of a chemical potential profile, the complete information on the electronic conductivity as a function of the activity can be determined. In contrast, for the evaluation of the electronic conductivity from the current–voltage relation, several measurements have to be performed, in order to obtain a complete $I$–$U$-graph. And since every single measurement may need an appreciable time for the attainment of the stationary state, the first method is much faster. An additional advantage, as becomes obvious from our experimental results, is the direct information on possible overvoltages at the electrodes and the possibility of excluding errors from ionic decomposition currents in the evaluation of the electronic conductivity.

### *2.2. Local potential probes in a heterogeneous transference cell*

In a cell Ag|AgBr|AgCl|Ag, both silver ions and electrons are transfered across the AgBr|AgCl interface (the anionic transference number is negligibly small). From experimental studies it is known that the very small electronic transference number of AgCl is about ten times larger than the electronic transference number of AgBr (see Table 1). This

Table 1
Conductivities of silver bromide and chloride at 300°C

| $\sigma_{300°C}$ $(\Omega\ cm)^{-1}$ | AgBr | AgCl |
|---|---|---|
| $\sigma_{Ag^+}$ | $3.59\times10^{-2}$ | $1.94\times10^{-3}$ |
| $\sigma_{e^-}$ | $1.85\times10^{-7}$ | $7.03\times10^{-8}$ |
| $t_{el}$ | $5.5\times10^{-6}$ | $3.6\times10^{-5}$ |
| $t_{Ag^+}$ | $\approx 1$ | $\approx 1$ |

difference in the transference numbers causes a discontinuity in the transport properties at the interface and, under current load, may lead to different consequences, depending on the boundary conditions (for an extensive treatment see Schmalzried and coworkers [5,6]). If no reaction is allowed to take place at the interface, a steady current through the cell will lead to the creation of a spatially varying potential profile. The direction of the current decides whether the chemical potential at the interface is higher or lower than its value at the electrode boundaries. If the interface is not coherent and thus allows reaction, a steady current leads to a continuous deposition of either the metal or the non-metal component (decomposition), again depending on the direction of the current. Fig. 5 shows a schematic representation for the AgBr | AgCl-phase boundary acting as a sink for silver, assuming a stationary state without any reaction at the interface. In this case, the silver flux is constant and independent of the position, $\xi$:

$$j_{Ag^+} = -L_{Ag^+}\nabla\tilde{\mu}_{Ag^+} = \text{const.} \qquad (11)$$

Thus, with activity-independent transport coefficients of the ions, $L_{Ag^+}$, the profiles of the electrochemical potential of the silver ions are linear within both electrolytes:

$$\nabla\tilde{\mu}_{Ag^+} = \text{const}, \qquad (12)$$

though the values of $\nabla\tilde{\mu}_{Ag^+}$ are different in both phases due to different ionic transport coefficients,

$$L_{Ag^+}(\text{AgBr}) > L_{Ag^+}(\text{AgCl}). \qquad (13)$$

Because both silver halides possess a high concentration of intrinsic defects, the chemical potential of the silver ions is assumed to be constant,

$$\nabla\mu_{Ag^+} = 0, \qquad (14)$$

and thus, from the definition of the electrochemical potential, $\tilde{\mu}_i = \mu_i + z_i F\varphi$, and eqs. (11) and (13), we obtain for the electrical potential:

$$\nabla\varphi = \text{const} \qquad (15)$$

in each phase. Fig. 6 shows a schematic plot of the discussed potentials across the heterogeneous cell. It

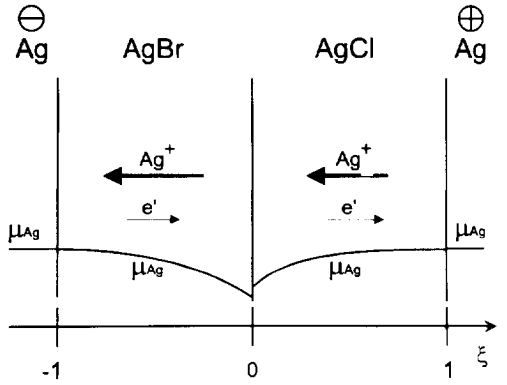


Fig. 5. Schematic representation of the transference cell Ag | AgBr | AgCl | Ag.

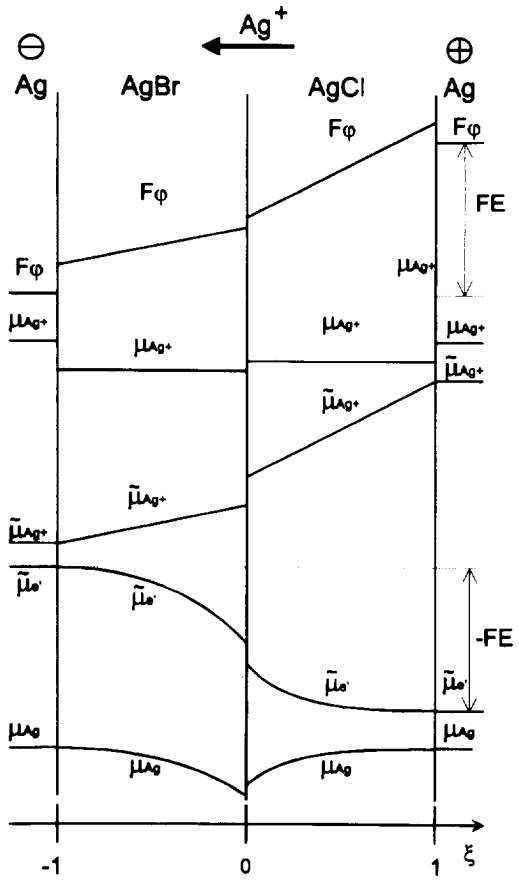


Fig. 6. Schematic profile of the (electro-)chemical potentials in the transference cell Ag | AgBr | AgCl | Ag.

has to be pointed out that all assumptions made for this refer to a AgBr | AgCl-interface. Since we measured an ionic overvoltage at the interface, a step of $\tilde{\mu}_{Ag^+}$ at the AgBr | AgCl-interface is already included in Fig. 6. A step of $\tilde{\mu}_{Ag^+}$ at the interface leads to a step in the chemical potential of silver at the interface, the magnitude of which also depends on a possible step of the electrochemical potential of electrons, $\tilde{\mu}_{e^-}$.

## 3. Experiments

### *3.1. Preparation of the polarization cell*

Silver bromide single crystals (Korth Kristallhandel, Kiel/Germany) were machined into rectangular shape ($9 \times 8 \times 5$ mm) and polished both mechanically and chemically, using an aqueous solution of $Na_2S_2O_3$. Each crystal was placed on a $30 \times 15 \times 2$ mm silica glass plate to which the platinum probes (with a diameter of 100 μm) and the two electrodes (platinum with a diameter of 100 μm; silver with a diamter of 150 μm) had been prefixed in a well defined geometry. On top of the AgBr-crystal a second silica glass plate was placed, and this sandwich-crystal was heated in a resistance furnace to the melting point of AgBr in order to embed the probes and the electrodes. The subsequent polarization experiments were carried out at a temperature of 300°C.

### *3.2. Circuit*

The schematic diagram in Fig. 1 shows the dc polarization cell equipped with probes for the measurement of the chemical potential profile. A constant potential difference $E_L$ between the two electrodes was applied with a potentiostat (Jaissle 100TB) and the voltage between the platinum probes and the silver cathode was measured with a digital multimeter (Keithley DMM 2001). The electronic current across the cell was determined by measuring the voltage drop at an ohmic resistance $R$ ($= 100$ kΩ) with a Keithley 2001 multimeter as well. All voltages were recorded via an IEEE-interface with a personal computer.

### *3.3. Preparation of the transference cell*

Two single crystals of AgBr and AgCl were machined into rectangular shape ($11 \times 4 \times 6$ mm) and polished both mechanically and chemically by an aqueous solution of $Na_2S_2O_3$. The two crystals were sintered together at their ($4 \times 6$ mm) surface at 380°C for three days. Silver probes were embedded in the assemblage at definite positions by heating silver wires (with a diameter of 150 μm) resistively. Two silver electrodes were fixed at the ends of the assemblage. The subsequent measurements were carried out at 300°C.

### *3.4. Circuit*

The schematic diagram in Fig. 5 shows the transference cell. A galvanostatic current was applied by means of a galvanostat. The probe signals were measured versus the silver cathode and recorded via an IEEE-interface.

## 4. Results

### *4.1. The polarization cell*

Fig. 7 shows typical measured local potential probe signals plotted versus their relative position $\xi$. The relation between the measured potential differ-

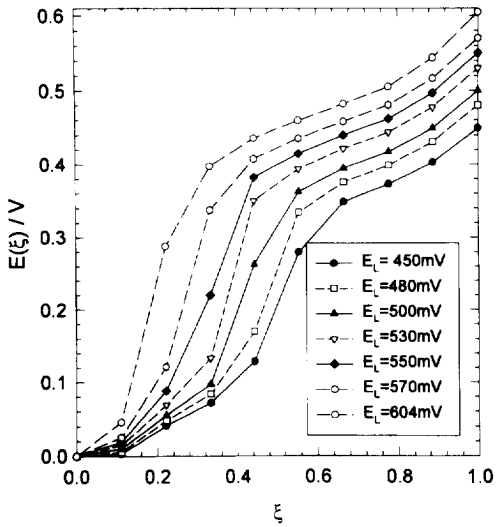


Fig. 7. Measured chemical potential profile in the polarization cell Ag | AgBr | Pt.

Table 2
Extrapolated potentials at the phase boundaries as expected by linear regression

| $I$ ($\mu$A) | $E(-\xi \rightarrow 1)$ Ag \| AgBr (mV) | $E(-\xi \rightarrow 0)$ AgBr \| AgCl (mV) | $E(\xi \rightarrow 0)$ AgBr \| AgCl (mV) | $E(\xi \rightarrow 1)$ AgCl \| Ag (mV) | $E_{cell}$ (mV) |
|---|---|---|---|---|---|
| 1 | 0.33 | −5.18 | −1.72 | 6.40 | 8.2 |
| 2 | 0.43 | −4.78 | −0.68 | 10.52 | 13.3 |
| 5 | 0.53 | −4.39 | 2.01 | 22.96 | 42.0 |
| 10 | 1.06 | −3.29 | 6.63 | 41.99 | 75.0 |
| 15 | 1.62 | −2.12 | 11.94 | 63.40 | 130.0 |

ence $E(\xi)$ and the chemical potential of silver as given by Eq. (9), reflects an increasing probe potential with decreasing silver activity. With increasing cell voltage $E_L$, an inflection point in the profile develops, which denotes a minimum in the electronic conductivity. At this minimum the electronic conduction changes from n- to p-type. In Fig. 8, the ratio of the externally measured current $i$ and the local gradient of $\tilde{\mu}_{e'}$ (derived from the slope of the $E(\xi)$-profile) is plotted versus the local silver activity.

Both figures illustrate several unexpected results. In Fig. 7, a deviation from the predicted $\mu_{Ag}$-profile is observed towards the platinum anode. Since the spatial resolution of the potential probes is not high enough, one cannot decide experimentally whether this deviation is due to a bulk effect, or whether it is caused by an overvoltage at the interface. In order to evaluate the electronic bulk conductivity, a polynomial fit of the measured profiles has been used. The resulting function has then been differentiated and divided by the respective polarization current, in

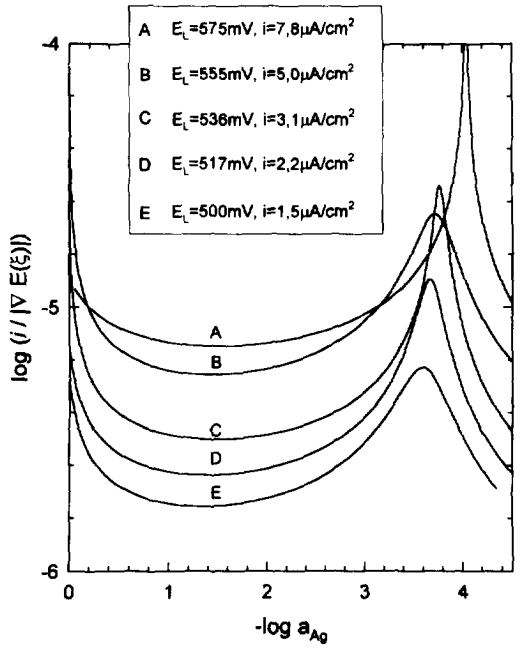


Fig. 8. Electronic conductivity plotted versus the bromine activity in AgBr at 300°C.

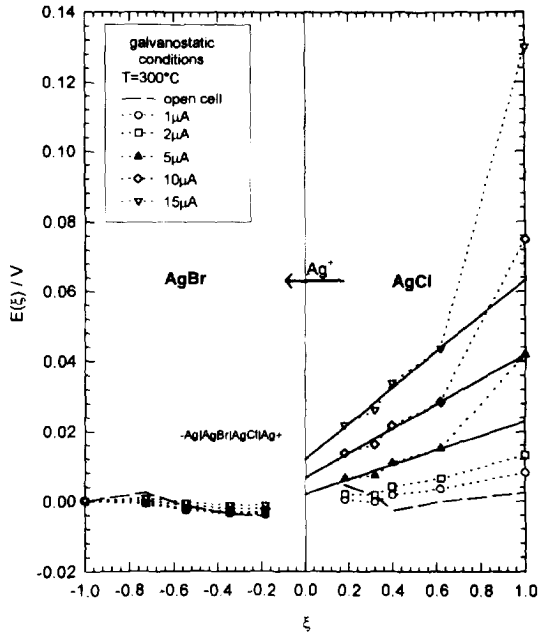


Fig. 9. Measured profile of the (electro-)chemical potentials in the transference cell Ag | AgBr | AgCl | Ag.

order to obtain the local electronic conductivities. As can be seen from Fig. 8, the resulting conductivities differ appreciably at different polarization voltages. In the next section, possible reasons for this observation are discussed.

### *4.2. The transference cell*

Fig. 9 shows the local electrochemical potentials of the silver ions measured with Ag-probes, plotted versus their position $\xi$ relative to the AgBr | AgCl phase boundary. The profile of the $\tilde{\mu}_{Ag^+}$-probes in the transference cell illustrates a larger driving force on the silver ions ($\nabla\tilde{\mu}_{Ag^+}$) in AgCl than in AgBr, as expected from their different conductivities. The small negative slope of $E(\xi)$ in AgBr is probably due to the existence of small temperature gradients across the cell which produce thermal voltages that are higher than the very small applied external voltages. The expected $\tilde{\mu}_{Ag^+}$-profile is linear within both electrolytes (Eq. (11)), and thus the measured profiles are extrapolated to the phase boundaries by linear regression (bold lines in Fig. 9; regression lines for 1 and 2 μA are calculated but not depicted). The regression lines reveal overpotentials for the silver ions at the AgBr | AgCl- and the AgCl | Ag-interface. Table 2 summarizes these extrapolated potential differences at the phase boundaries. The overpotential at the AgBr | AgCl-interface is related linearly to the current density across the cell as shown in Fig. 10.

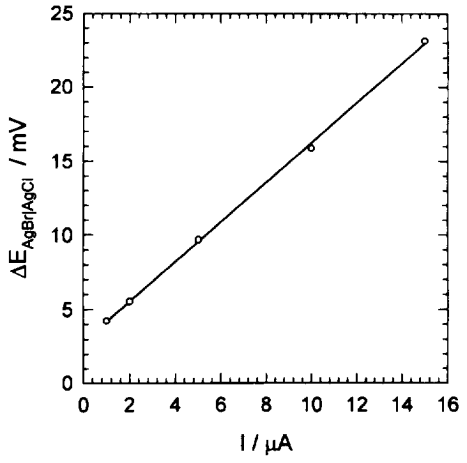


Fig. 10. Overpotential at the AgBr | AgCl interface versus current density in the transference cell.

## 5. Discussion

### *5.1. The polarization cell*

Two main aspects of the reported measurements have to be emphasized. As has already been shown by Mizusaki and Fueki [4], the use of local probes in a polarization cell allows a much faster access to the (activity dependent) electronic conductivity than conventional two-electrode cells. In addition, inherent errors in the quantitative determination due to the existence of interfacial overvoltages can be avoided. In the present case, the observed profiles show a reproducible deviation from the expected profiles within the anode region. To date, no comparable observations have been reported in the literature. Mizusaki and Fueki [4], who studied the partial electronic conductivity of silver halides in polarization cells Ag | AgX | C using local probes, did not report any overvoltages. This is probably due to the fact that they used only four probes, which made it correspondingly more difficult to detect deviations from theoretical profiles. However, a closer inspection of the experimental results reported in [4] indicates that Mizusaki and Fueki probably overlooked the existence of an electronic overvoltage at the AgBr | C-interface.

As already pointed out above, on the basis of the present results it is difficult to comment unequivocally on the deviation from the theoretical predictions. One may interprete this deviation either as the existence of a second inflection point in the potential distribution at high potentials, or as the result of an overvoltage at the interface. In the following, these two possible causes for the deviation will be discussed.

### *5.2. Kinetic effects at the AgBr | Pt interface*

If one assumes negligible electron conduction in the p-type conducting part of the crystal (see also Fig. 7), the local current density can be described simply by Eq. (2). Extrapolation of the p-conducting

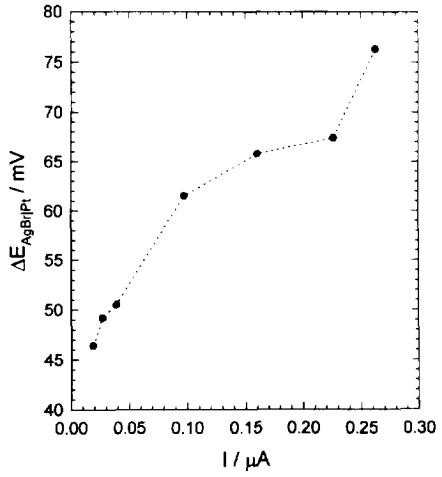


Fig. 11. Overpotential at the AgBr | Pt interface versus electronic current density in the polarization cell.

branch to the AgBr | Pt-interface leads to an appreciable difference relative to the cell voltage $E_L$. In Fig. 11, this difference is plotted as an electronic overvoltage at the AgBr | Pt interface versus the electronic current density across the cell. Despite the strong scattering of the data points, it can be concluded that the relation between the current density and the overvoltage is non-ohmic. For the interpretation of this behaviour, at least two different ideas may be taken into account.

(1) Perhaps the most obvious explanation is related to the decomposition of silver bromide at the anode, which should lead to the formation of bromine in pores at the AgBr | Pt interface by the decomposition reaction

$$Br_{Br}^{\times} + V_{Ag}' + h^{\cdot} = \tfrac{1}{2}Br_2, \qquad (16)$$

where the Kröger–Vink-notation has been used. Any decomposition of the specimen, according to Eq. (16), causes a decreasing contact area between silver bromide and platinum and, thus, results in an increasing resistance for the electronic charge carriers. Thermodynamically, the decomposition of AgBr can take place even at small polarization voltages. In practice, the decomposition depends on the construction and the geometry of the blocking electrode. Große and Schmalzried [12] demonstrated that the bromine component can leave the crystal not only at triple contacts between the compound AgBr, the metal electrode and the gas phase. Rather, it may also leave the crystal by evaporation from free surfaces of the compound in the vicinity of the electrode, thus producing visible etch pits. However, if the gas phase has access to the contact AgBr | Pt, the direct production of bromine at this point will be more effective. Unfortunately, the detection of small decomposition currents beside the electronic polarization current is difficult. Große [14] successfully used thin silver wires, embedded in the polarization cell, as potential probes for the detection of ionic transient currents during the relaxation of cells after a change of the polarization voltage. In principle, such silver probes should also detect ionic decomposition currents. But a simple estimation shows that the resulting voltage signals are probably much too small to be measured reliably. Neglecting diffusion potentials, the voltage signal between two silver probes which is due to a silver ion flux, is given by:

$$\Delta E = \frac{1}{F} \cdot \Delta \tilde{\mu}_{Ag^+} = -\frac{i_{Ag^+} \cdot \Delta x}{\sigma_{Ag^+}}. \qquad (17)$$

Using an ionic conductivity of $\sigma_{Ag^+} \approx 0.01$ $(\Omega\mathrm{cm})^{-1}$ and assuming an ionic current density of $i_{Ag^+} \approx 0.1$ μA, a voltage signal of approximately $\Delta E \approx 10$ μV results between two silver probes at a distance of 1 cm. Since this voltage may be of the order of the neglected diffusion potentials, and since any small temperature difference along the polarization cell may cause a much larger thermovoltage, it will be almost impossible to reliably detect the voltage, which is due to an ionic decomposition current. In this respect, the difference between the conductivities in Fig. 8, which have been determined from individual potential profiles measured at different polarization voltages, is interesting. The profiles themselves cannot be influenced by ionic currents, since platinum probes only detect the driving force for electronic fluxes. In other words, the only reason for the differing results from different polarization voltages may come from an erroneous determination of the electronic current density. Obviously, the most critical error source in the electronic current measurement is the occurrence of a superposed ionic decomposition current. In the external circuit, an ionic contribution cannot be distinguished from the electronic current, thus it only increases the experi-

mental total current. Consequently, in the calculation of the electronic conductivities, an ionic current leads to the determination of conductivity values which are too large. Additionally, one would expect that this disturbance increases with increasing polarization voltage, due to an increasing decomposition of the electrolyte. This effect can clearly be seen from Fig. 8 in the present case. Thus, the use of local electronic probes not only may show the existence of overvoltages at the electrodes, but indirectly also allows the detection of ionic decomposition currents.

(2) A second explanation for the non-linear behaviour of the blocking electrode may be the formation of a Schottky-contact. Thus, one may speculate on the existence of a depletion layer for electronic charge carriers next to the platinum anode. This depletion layer could rectify the electronic charge carriers in the cell, giving rise to an exponential current–voltage behaviour.

(3) Another mechanism which might disturb the electronic transfer at the anode could be the growth of a high resistance interphase. In the present case, this would probably mean the formation of a platinum bromide layer.

### 5.3. *Bulk effects*

As already mentioned above, a deviation from the expected profile could also arise from a bulk effect, i.e. from a decrease of the hole conductivity with decreasing silver activity at very low silver activities. In this case, a continuous deviation of the profile within the bulk should be obtained. Unfortunately, the spatial resolution of our probes is not high enough to decide whether this is really the case.

One may speculate that at very low silver activities the increasing hole concentration, in accordance with an increasing cation vacancy concentration, may lead to an association of vacancies and holes (trapping), thus forming neutral associates. However, such a reaction would influence the hole conductivity, but could not explain a maximum in the hole conductivity. Only in combination with an additional strong decrease of the mobility of untrapped electron holes, a conductivity maximum could be explained.

As Riess and others [15–17] demonstrated, the strong increase in the cation defect concentration at very high polarization voltages may lead to the failure of the conventional Wagner–Hebb analysis. As a result, the slope of the (log $i$ versus $E$)-graph in the p-type conducting dominated branch should change to half the value predicted by Eq. (2). It is obvious, that the profile of the chemical potential of the metal component (i.e. the electrochemical potential of the electrons) is not necessarily influenced by this effect, as long as the blocking condition, $j_{A^+} = 0$, is fulfilled, and the changes of the ionic defect structure do not influence the electronic conductivity. Under ideal blocking conditions, $\nabla\tilde{\mu}_{A^+} = 0$, thus $\nabla\mu_A = \nabla\tilde{\mu}_{e^-}$, even if $\nabla\mu_{A^+} \neq 0$. Any change of the profile of $\nabla\mu_A$ can only be caused by a change of the electronic conductivity, i.e. the electronic defect structure.

The aforementioned arguments show that in the present state no definite conclusion can be drawn on the cause of the deviation in the potential profile from the results predicted by the ideal transport behaviour. However, the most probable interpretation of our experimental observations is based on an electronic overvoltage due to a growing morphological change of the blocking electrode with increasing polarization voltage. This morphological change might be caused by a continuous decomposition of the solid electrolyte, even at low polarization voltages. The results in Fig. 8 provide strong evidence for a continuous decomposition at the blocking interface. An interesting question, which remains unanswered in the present instance, concerns the reproducibility and reversibility of the interfacial structure changes. Further experimental work, focussing on the preparation of well-defined interface structures and the control of these structures during the electrochemical polarization, will be performed.

### 5.4. *The transference cell*

The measured overpotential at the AgBr | AgCl-interface is related linearly to the current density across the transference cell (see Fig. 10). Thus, the AgBr | AgCl-interface, prepared by sintering as described above, forms an ohmic resistance in the electrical circuit. Assuming conventional electrode kinetics for the ion exchange, an equilibrium exchange flux density, $i_0$, can be derived from Fig. 10, in line with the Butler–Volmer-formalism, from Fig.

10. For a small overvoltage at the interface the Butler–Volmer-equation.

$$i_{el} = i_{e^-} - i_{h^\cdot} = i_0 \left[ \exp\left( \frac{\alpha z F \Delta E}{RT} \right) - \exp\left( - \frac{(1-\alpha) z F \Delta E}{RT} \right) \right] \quad (17)$$

simplifies to

$$i_{el} = i_0 \frac{z F \Delta E}{RT} \quad (18)$$

resulting in an exchange current density of $i_0 \approx 0.4$ mA cm$^{-2}$. In comparison to the only other value for an exchange current density between two solid ionic conductors ($Ag_2S|AgI$), which to our knowledge has been reported [3], this value is smaller by more than three orders of magnitude. Before we undertake serious attempts for an interpretation of this result, it seems necessary to perform similar experiments on specimens with well defined interfaces. Thus, in continuation of the present study, future experimental work will be dedicated to the preparation of chemically clean and structurally well defined interfaces between different ionic conductors.

## 6. Conclusions

The aim of the present study was to emphasize the importance of interface kinetics for a complete description of many non-equilibrium processes in the solid state and to demonstrate the usefulness of local electrochemical probes. Thus, as a first example, we studied the Wagner–Hebb polarization cell which was originally developed for the quantitative investigation of partial electronic conductivities in mixed conductors. Until now the possible influence of interface processes on the quantitative evaluation was nearly always neglected. Only recently, Riess [18,19] pointed out this fact and proposed an experimental method which avoids a disturbance of quantitative measurements by interface kinetics. In the present case we could show that an electronic overvoltage at high polarization voltages may exist at the blocking electrode, invalidating the conventional analysis.

The second experiment was related to the functioning of interfaces between two different solid electrolytes during electric current load. Often, mixed conducting layers are used as electrodes on solid electrolytes to improve the exchange kinetics with molecular oxygen from the gas phase. Since both materials generally exhibit different partial conductivities, their interface may suffer from internal reactions during current load as has been discussed by Schmalzried and Backhaus-Ricoult [5]. It is obvious that any overvoltage for the exchange of charge carriers at the interface will influence the kinetics of these reactions.

To decide whether interface kinetics or bulk effects cause the deviations in the potential profile of the Wagner–Hebb-cell, an experiment with better spatial resolution of the probes close to the platinum anode is necessary. Therefore we plan to apply microlithographic techniques for the preparation of probe geometries with better spatial resolution.

## Acknowledgements

We are grateful to Prof. H. Schmalzried for his support and stimulating suggestions. One of us (J.J.) is grateful to the Fonds der Chemischen Industrie (Germany) for financial support.

## References

[1] H. Schmalzried, Chemical Kinetics of Solids (VCH, Weinheim, 1995).
[2] D. Hoeschen, Ph.D. Thesis (Georg-August University of Göttingen, Göttingen, 1966).
[3] H. Schmalzried, M. Ullrich and H. Wysk, Solid State Ionics 51 (1992) 91.
[4] J. Mizusaki and K. Fueki, Rev. Chim. Min. 17 (1980) 356.
[5] H. Schmalzried and M. Backhaus-Ricoult, Prog. Solid State Chem. 22 (1993) 1.
[6] U. Stilkenböhmer, Ph.D. Thesis (University of Hannover, Hannover, 1994).
[7] I. Riess, J. Electrochem. Soc. 139 (1992) 2250.
[8] C. Wagner, Proc. Intern. Committee Electrochem. Thermodyn. Kinetics (CITCE) 7 (1955) 361.
[9] M. Hebb, J. Chem. Phys. 20 (1952) 185.
[10] B. Ilschner, J. Chem. Phys. 28 (1958) 1109.
[11] I. Riess, 2nd Intern. Symp. Ionic and Mixed Conducting Ceramics, 185th Electrochem. Soc. Meeting (San Francisco, 1994).
[12] T. Große and H. Schmalzried, Z. Phys. Chem. (NF) 172 (1991) 197.

[13] R.C. Hanson, J. Phys. Chem. 66 (1962) 2376.
[14] T. Große, Ph.D. Thesis (University of Hanover, 1991).
[15] I. Riess, Solid State Ionics 66 (1993) 331.
[16] R.A. Montani and J.C. Bazán, Solid State Ionics 46 (1991) 211.
[17] R.A. Montani and J.C. Bazán, J. Phys. Chem. Solids 50 (1989) 1207.
[18] I. Riess and R. Safadi, Solid State Ionics 59 (1993) 99.
[19] I. Riess, Solid State Ionics 51 (1992) 219.